A wearable DC tribovoltaic power textile woven by P/N-type organic semiconductor fibers

Beibei Fan [a,c], Guoxu Liu [a,b], Yiming Dai [a,c], Zefang Dong [a,b], Ruifei Luan [a,b], Likun Gong [a,b], Zhi Zhang [a,b], Zhong Lin Wang [a,b,d,e], Chi Zhang [a,b,c] *

[a] *CAS Center for Excellence in Nanoscience, Beijing Key Laboratory of Micro-nano Energy and Sensor, Beijing Institute of Nanoenergy and Nanosystems, Chinese Academy of Sciences, Beijing 101400, China*

[b] *School of Nanoscience and Technology, University of Chinese Academy of Sciences, Beijing 100049, China*

[c] *Center on Nanoenergy Research, School of Physical Science and Technology, Guangxi University, Nanning, 530004, China*

[d] *Georgia Institute of Technology, Atlanta, GA, USA*

[e] *Guangzhou Institute of Blue Energy, Knowledge City, Huangpu District, Guangzhou 510555, China*

* Corresponding author at: Tribotronics Research Group, Beijing Institute of Nanoenergy and Nanosystems, Chinese Academy of Sciences

E-mail addresses: czhang@binn.cas.cn (C. Zhang)

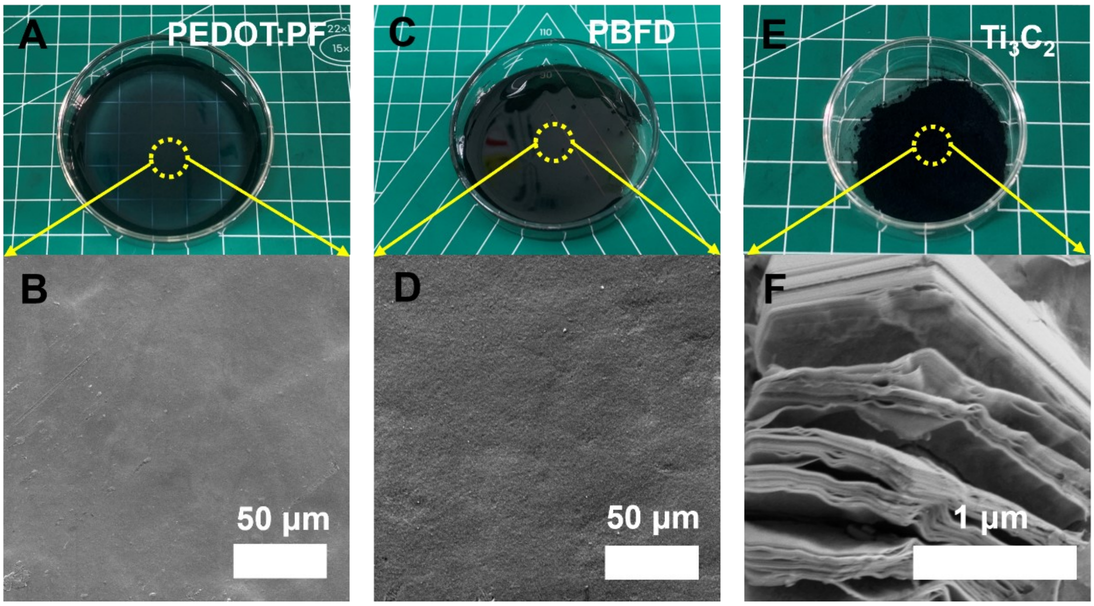

Fig. S1｜ (A, B) PEDOT:PF solution and SEM image of PEDOT:PF. (C, D) PBFD solution and SEM image of PBFD. (E, F) Ti_3C_2 powder and SEM image of Ti_3C_2.

Fig. S2｜(A) Ti_3C_2@CFs fibers. (B) PEDOT:PF@Ti_3C_2@CFs fibers. (C) PBFD@CFs fibers.

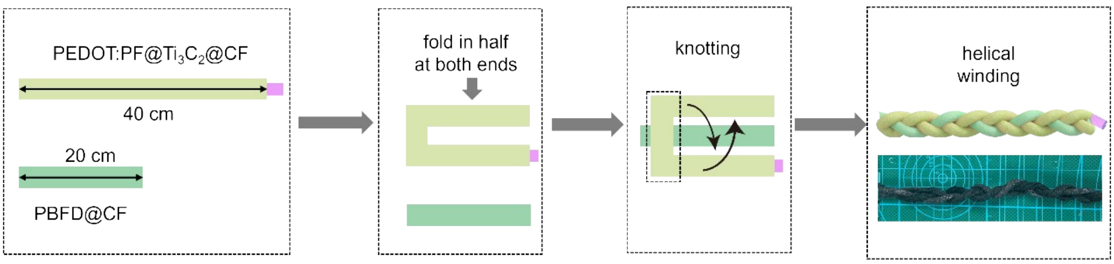

Fig. S3｜The weaving manufacturing process of SFs.

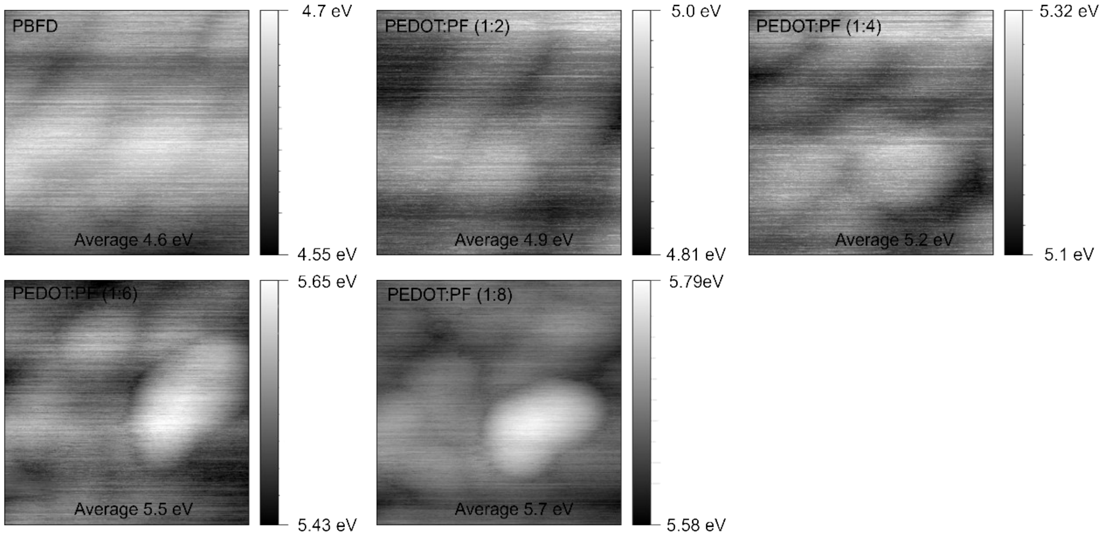

Fig. S4 | Work function measurements of PBFD and PEDOT:PF from KPFM tests.

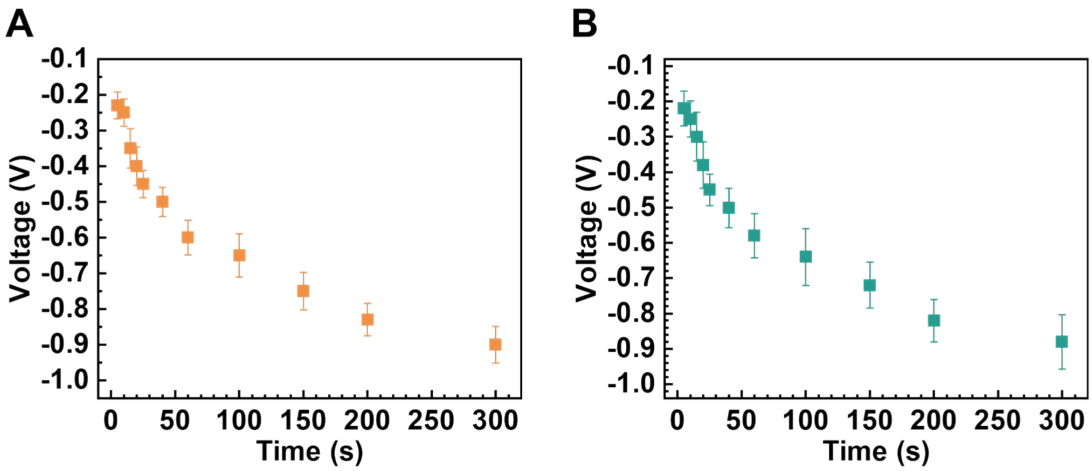

Fig. S5 | **(A)** The surface potential of of PEDOT:PF in sliding state. **(B)** The surface potential of of PEDOT:PF in compression state.

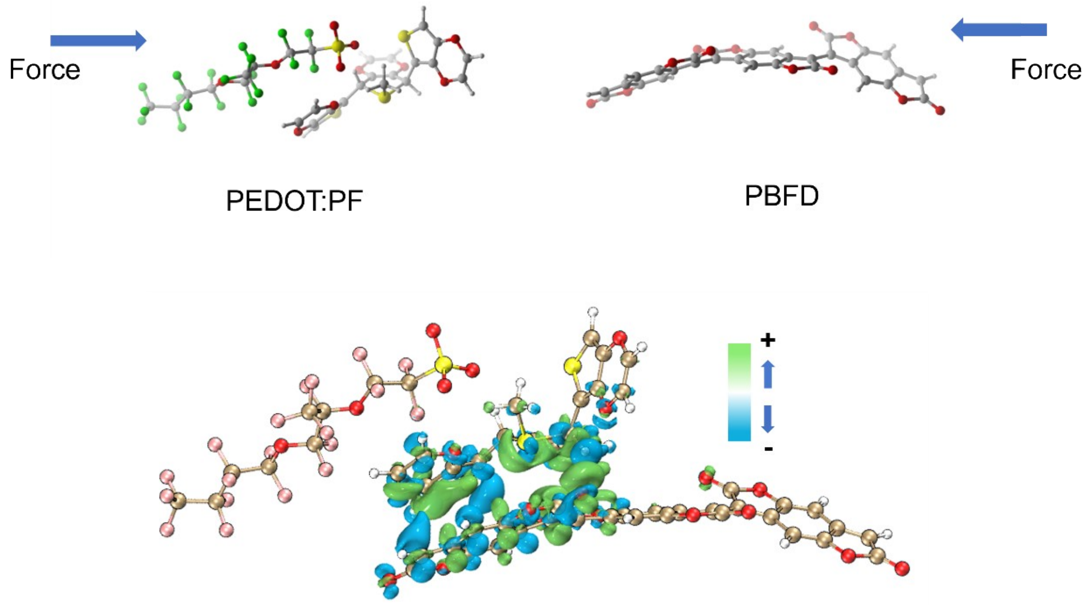

Fig. S6 | The distribution of gain and loss electrons at the interface between PBFD and PEDOT:PF molecules.

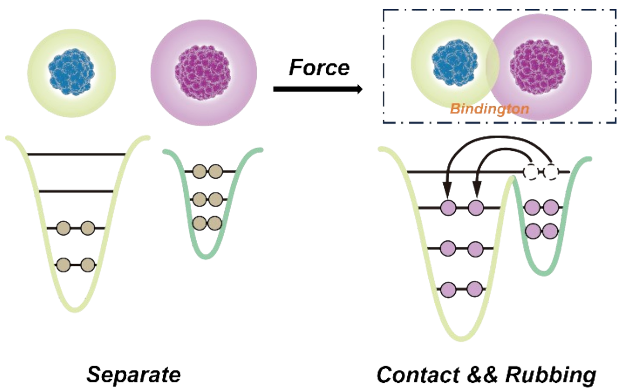

Fig. S7 | Electron-cloud-potential-well model of the electron transition process and the release of ‘‘bindington’’ as the excitation energy of the tribovoltaic effect.

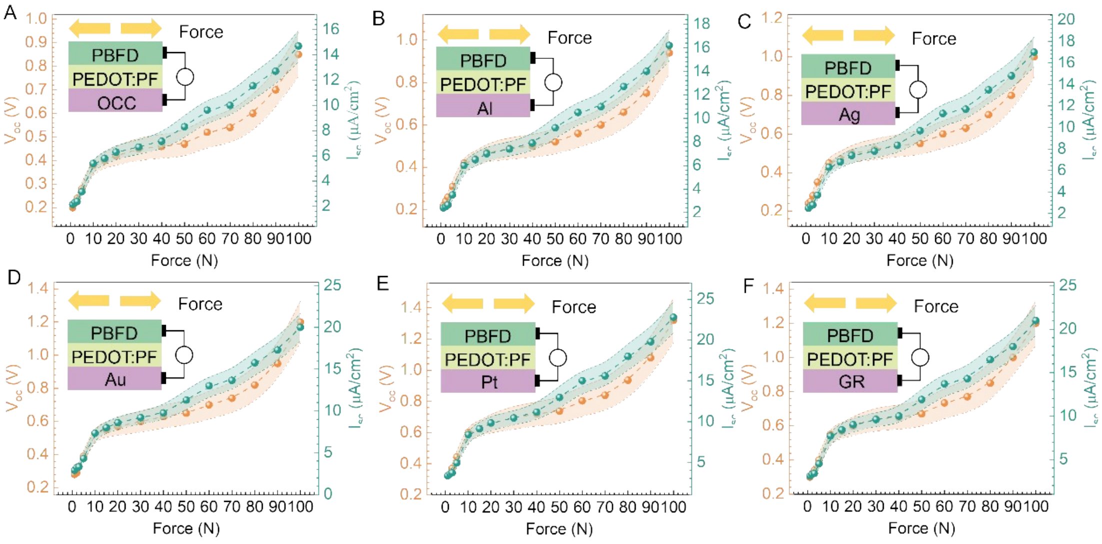

Fig. S8 | V_{oc} and I_{sc} of sliding mode generated by PEDOT:PF/PBFD interface under different materials.

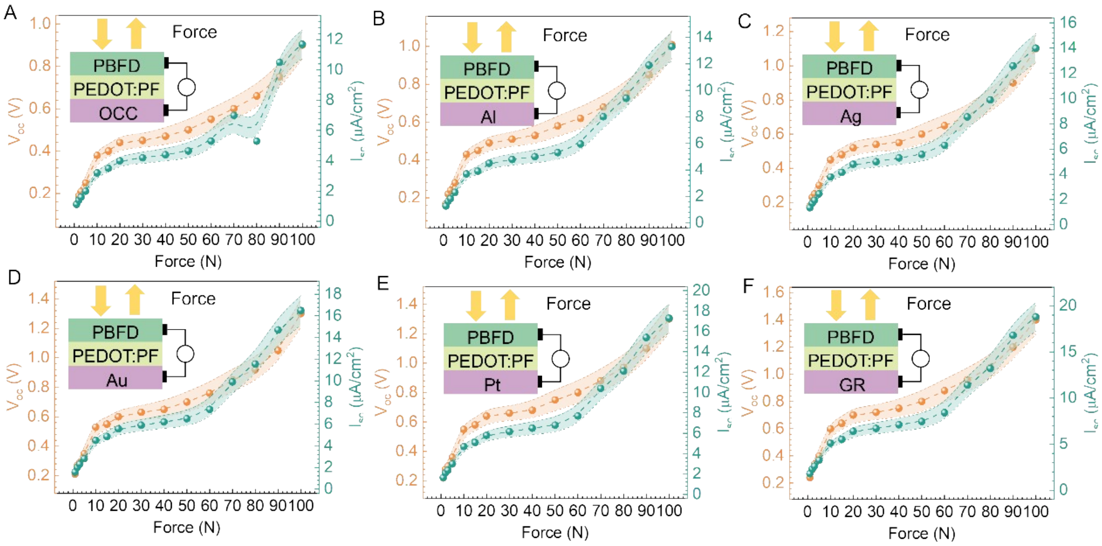

Fig. S9 | V_{oc} and I_{sc} of compression mode generated by PEDOT:PF/PBFD interface under different materials.

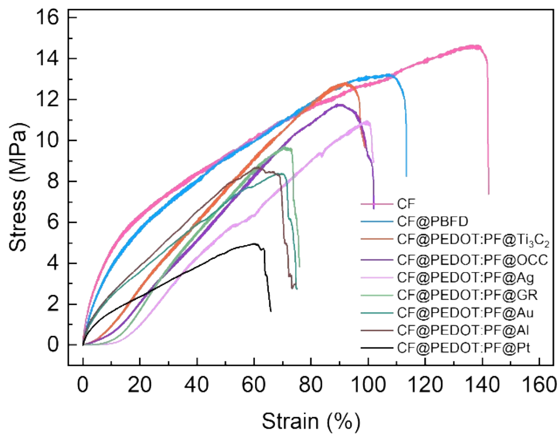

Fig. S10 | The tensile-strain curves of different fibers.

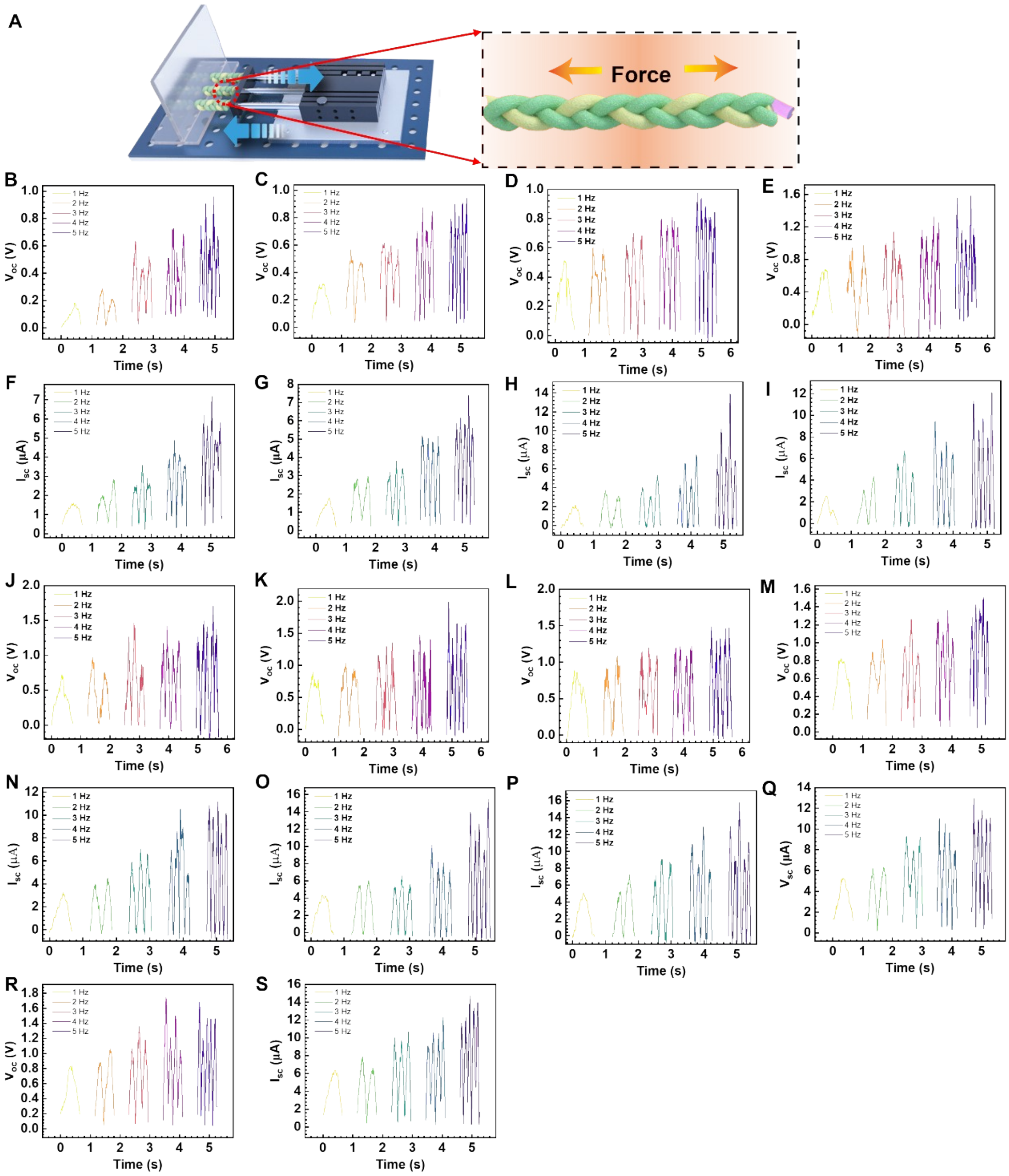

Fig. S11 | (A) Schematic diagram of SFs electrical output tested in the tensile state. (B, F) The V_{oc} and I_{sc} of SFs based 0.2 mm CFs. (C, G) The V_{oc} and I_{sc} of SFs based 0.5 mm CFs. (D, H) The V_{oc} and I_{sc} of SFs based 1 mm CFs. (E, I) The V_{oc} and I_{sc} of SFs based 2 mm CFs. (J, N) The V_{oc} and I_{sc} of SFs based 3 mm CFs. (K, O) The V_{oc} and I_{sc} of SFs based 4 mm CFs. (L, P) The V_{oc} and I_{sc} of SFs based 5 mm CFs. (M, Q) The V_{oc} and I_{sc} of SFs based 7 mm CFs. (R, S) The V_{oc} and I_{sc} of SFs based 10 mm CFs.

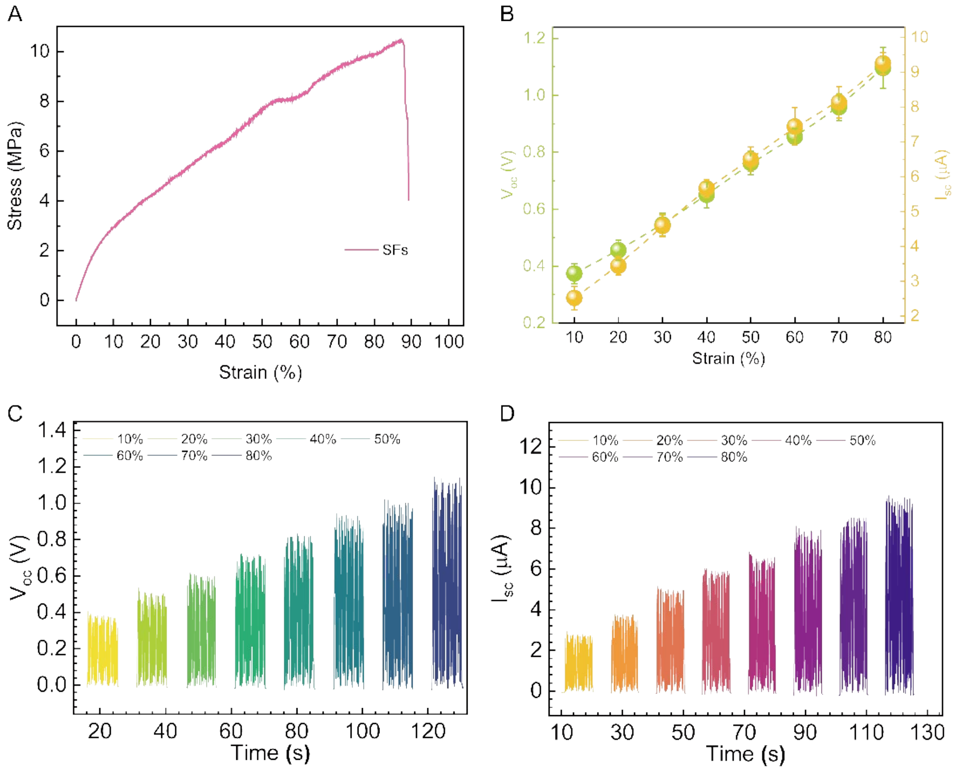

Fig. S12 | (A) The tensile-strain curves of SFs. (B- D) The V_{oc} and I_{sc} of SFs at 10-80% -strain.

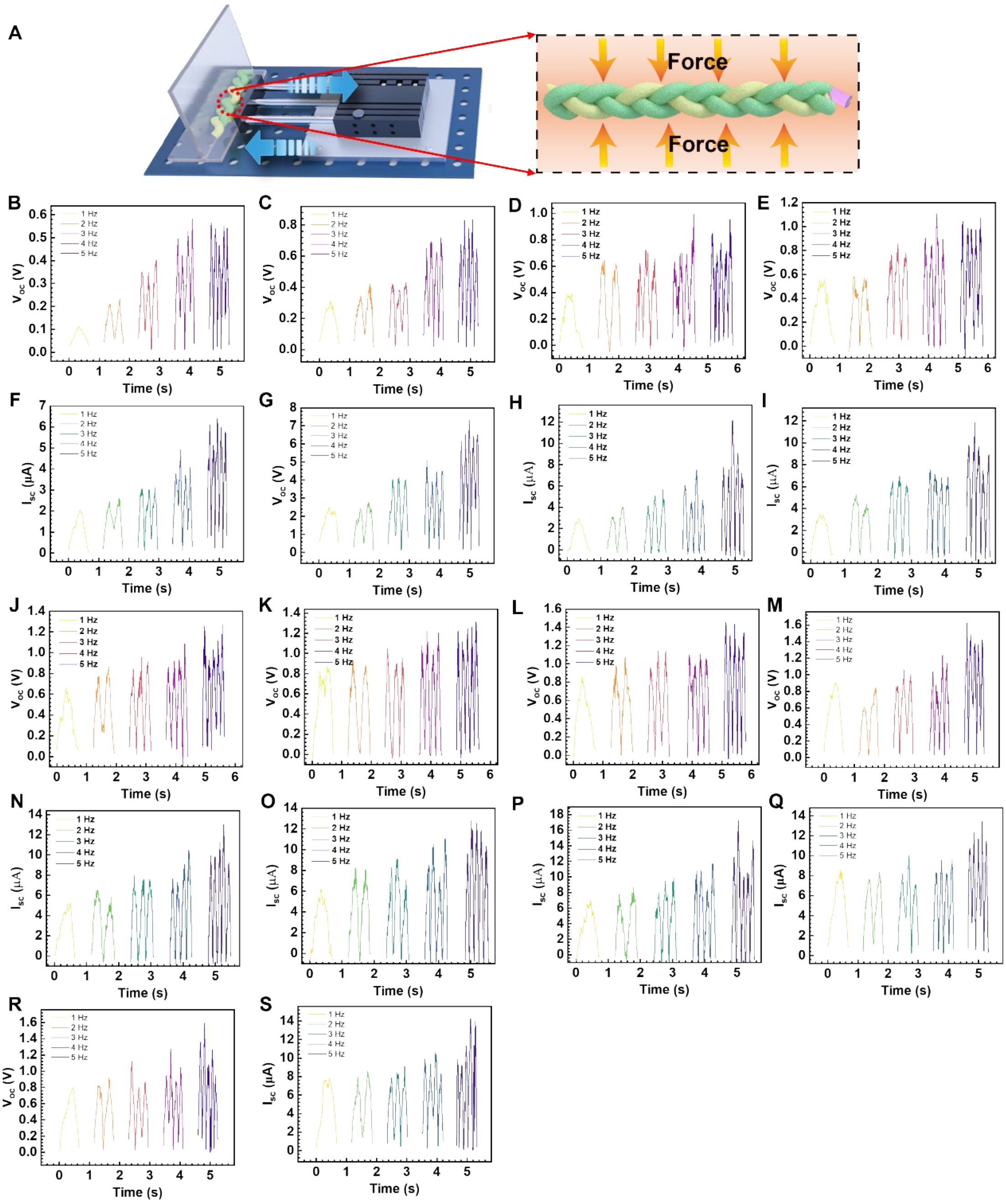

Fig. S13 | (A) Schematic diagram of SFs electrical output tested in the compression state. (B, F) The V_{oc} and I_{sc} of SFs based 0.2 mm CFs. (C, G) The V_{oc} and I_{sc} of SFs based 0.5 mm CFs. (D, H) The V_{oc} and I_{sc} of SFs based 1 mm CFs. (E, I) The V_{oc} and I_{sc} of SFs based 2 mm CFs. (J, N) The V_{oc} and I_{sc} of SFs based 3 mm CFs. (K, O) The V_{oc} and I_{sc} of SFs based 4 mm CFs. (L, P) The V_{oc} and I_{sc} of SFs based 5 mm CFs. (M, Q) The V_{oc} and I_{sc} of SFs based 7 mm CFs. (R, S) The V_{oc} and I_{sc} of SFs based 10 mm CFs.

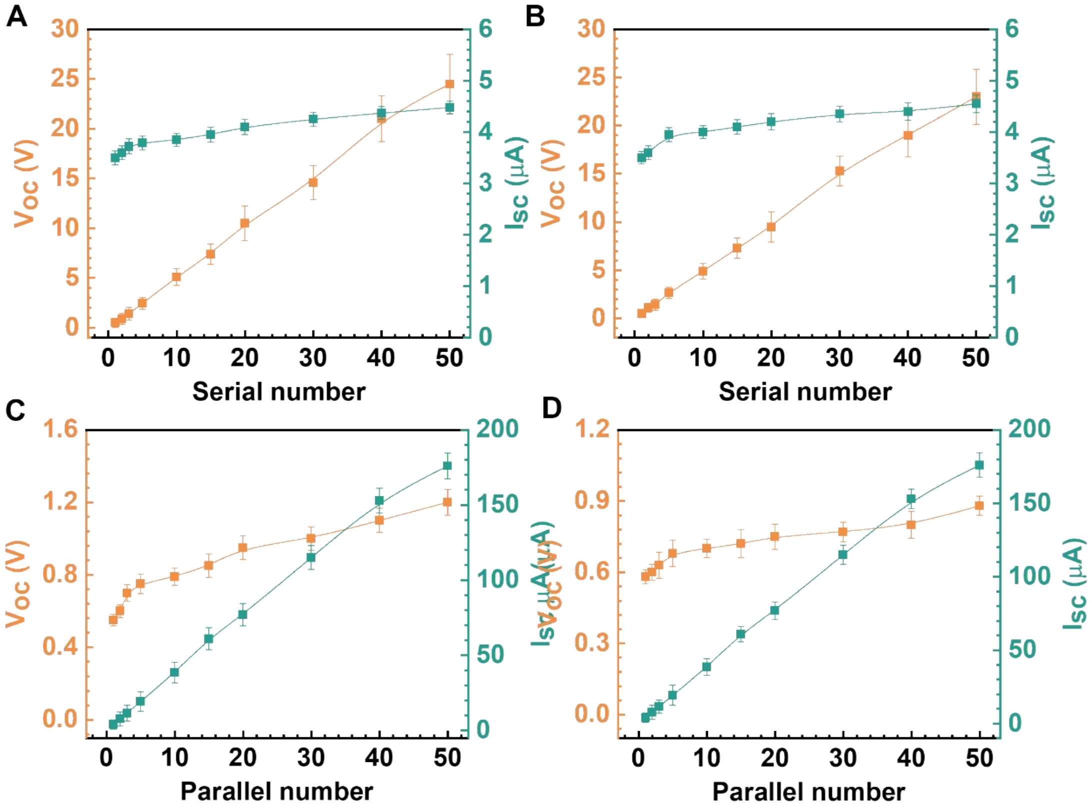

Fig. S14｜ (A, B) The Serial V_{oc} and I_{sc} of SFs in in the tensile state and compression state. (C, D) The Parallel V_{oc} and I_{sc} of SFs in in the tensile state and compression state.

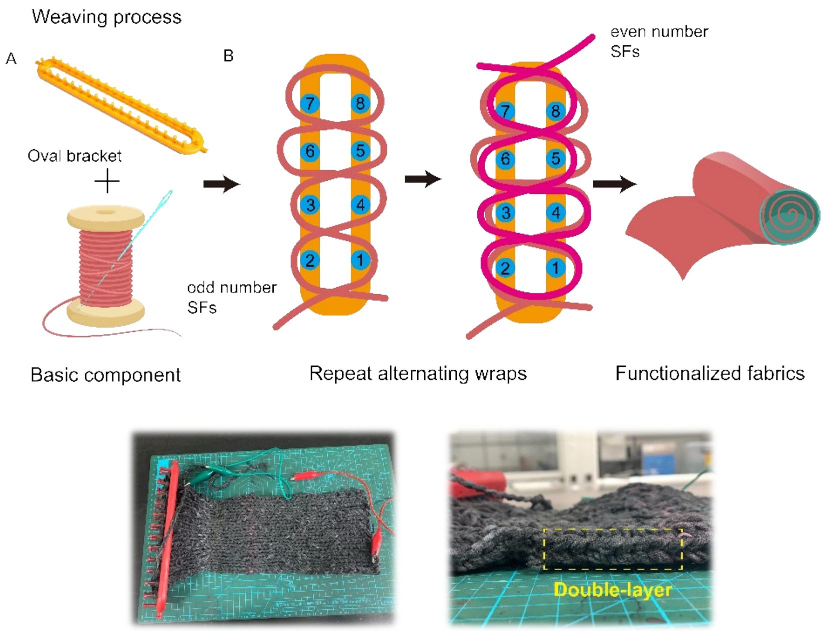

Fig. S15｜ The weaving manufacturing process of WDPs.

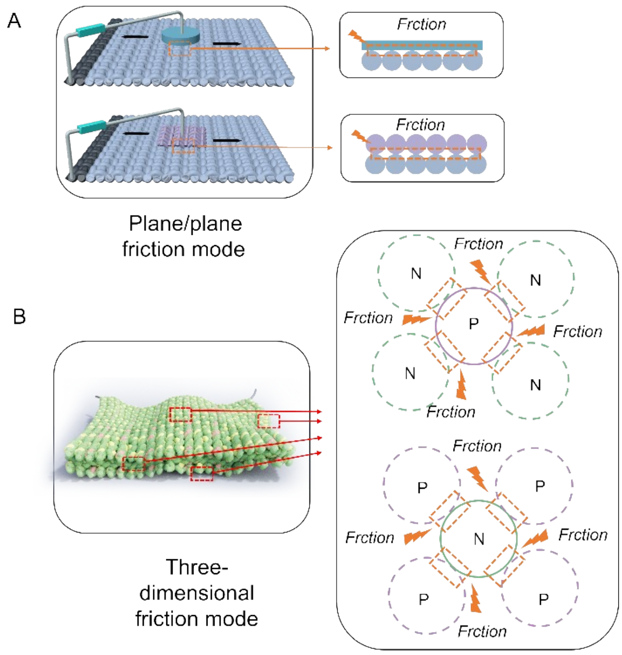

Fig. S16 | Comparison of plane/plane mode and three-dimensional friction mode

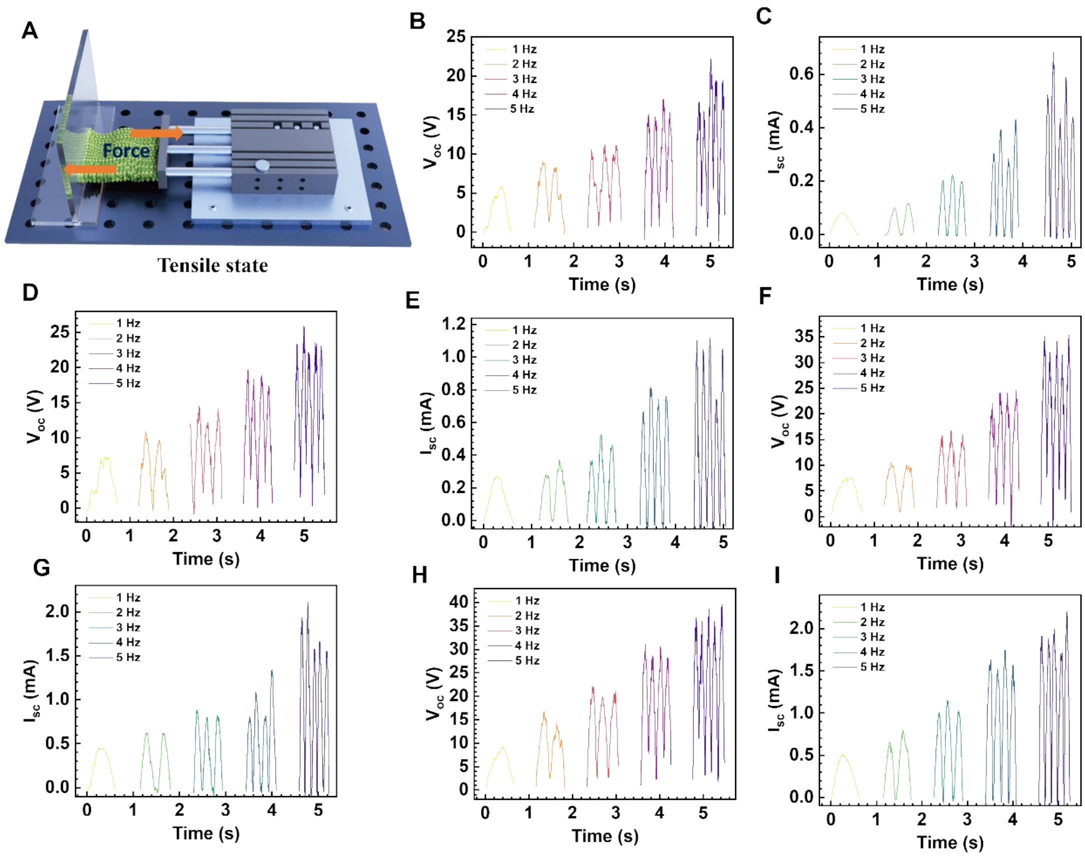

Fig. S17 | **The V_{oc} and I_{sc} of WDPs in tensile state.** (A) Schematic diagram of WDPs electrical output tested in the tensile state. (B, C) The V_{oc} and I_{sc} of 5×10 cm^2 WDPs. (D, E)The V_{oc} and I_{sc} of 10×10 cm^2 WDPs. (F, G) The V_{oc}

and I_{sc} of 10×20 cm^2 WDPs. (H, I) The V_{oc} and I_{sc} of 10×30 cm^2 WDPs.

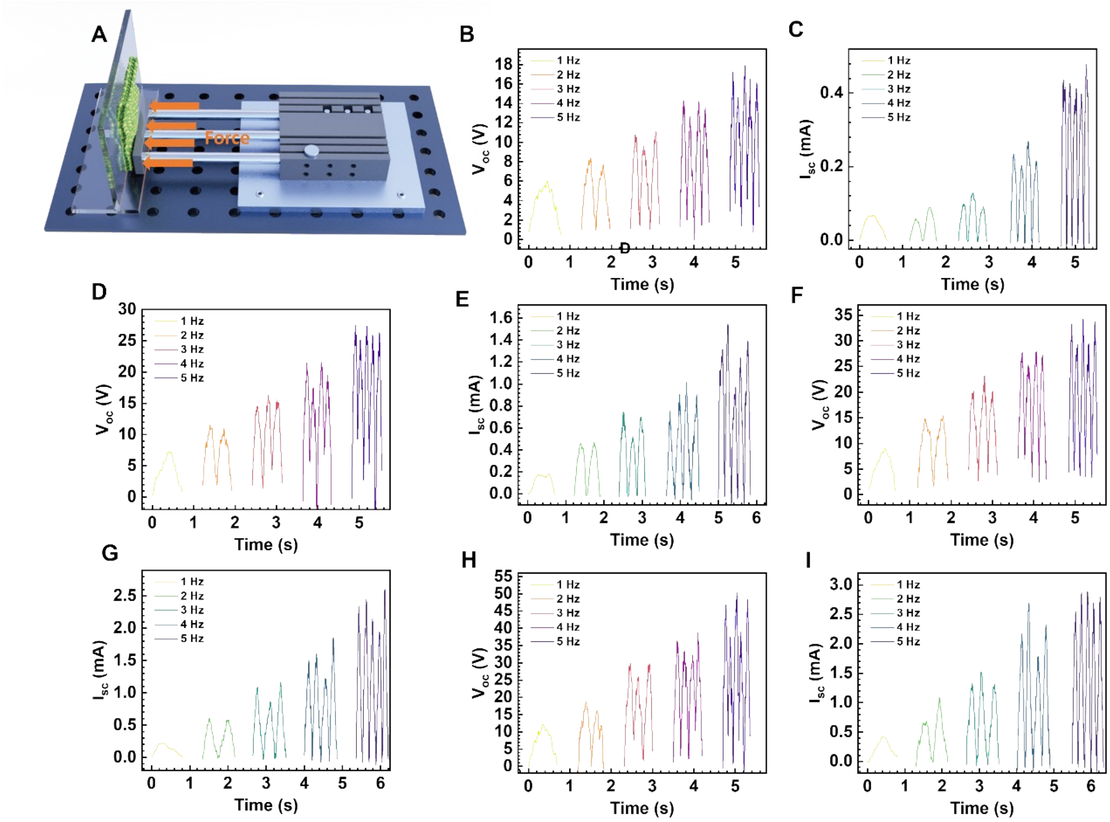

Fig. S18 | The V_{oc} and I_{sc} of WDPs in compression state. (A) Schematic diagram of WDPs electrical output tested in the compression state. (B, C) The V_{oc} and I_{sc} of 5×10 cm^2 WDPs. (D, E) The V_{oc} and I_{sc} of 10×10 cm^2 WDPs. (F, G) The V_{oc} and I_{sc} of 10×20 cm^2 WDPs. (H, I) The V_{oc} and I_{sc} of 10×30 cm^2 WDPs.

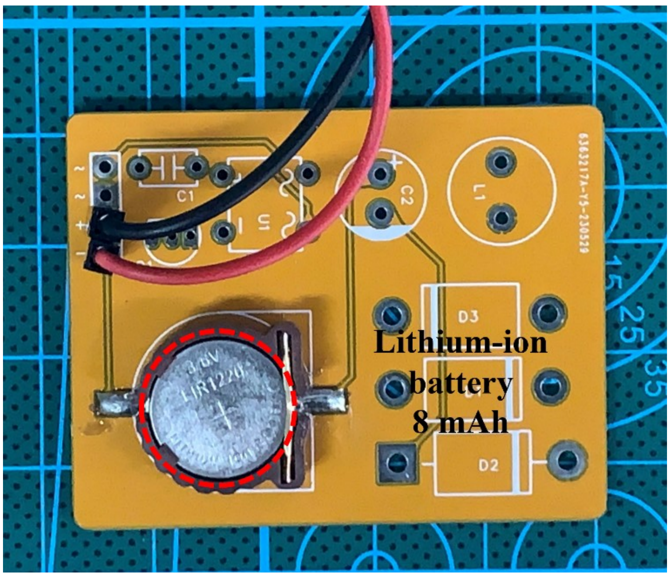

Fig. S19 | The Lithium-ion battery device.

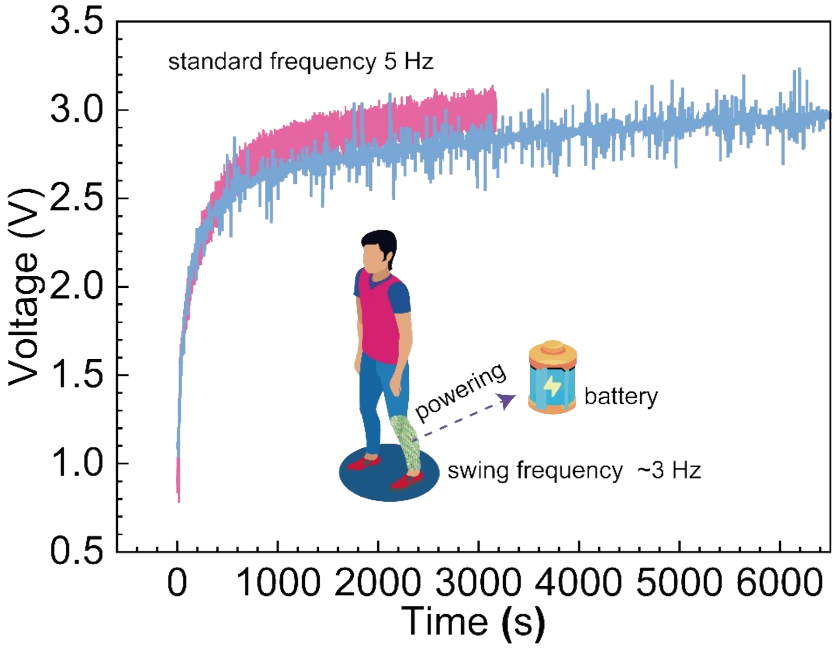

Fig. S20 | Comparison of the charging of batteries by the kinetic energy collected by WDP at 5Hz and the charging of batteries by collecting normal human kinetic energy

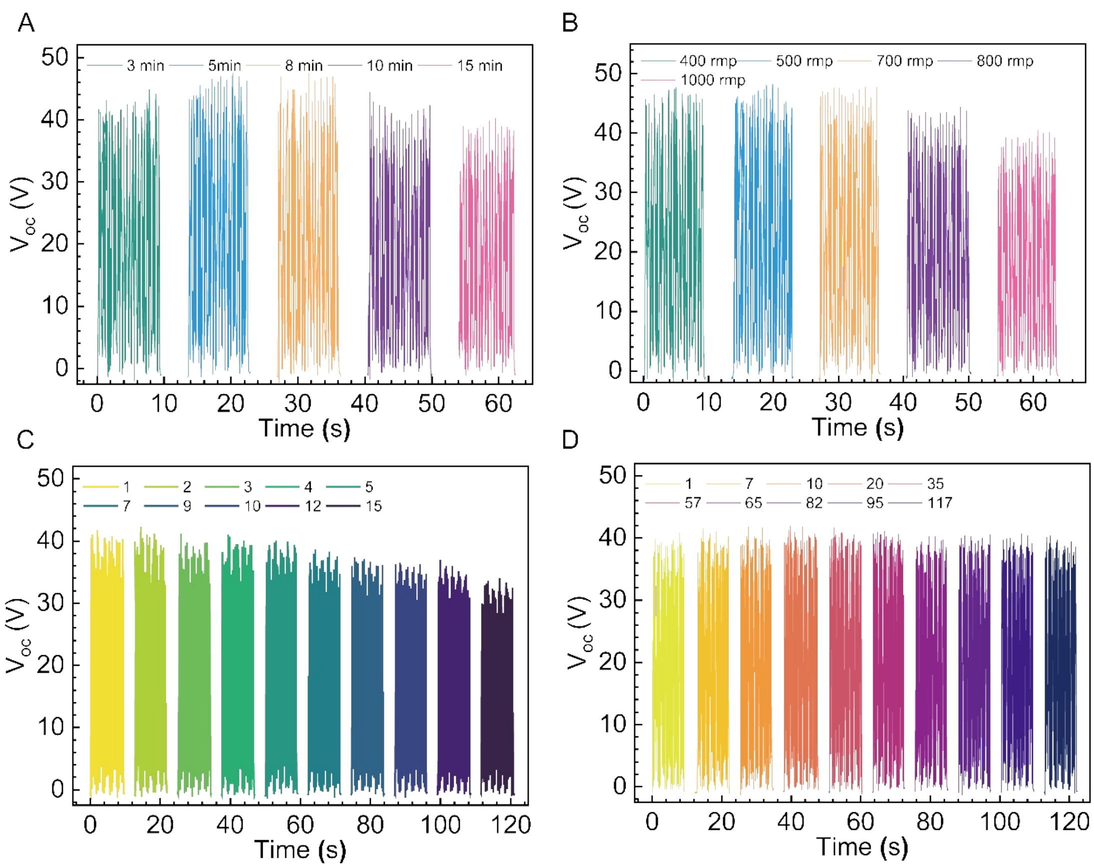

Fig. S21 | The investigation of WDPs' cycle washability and long-term durability.

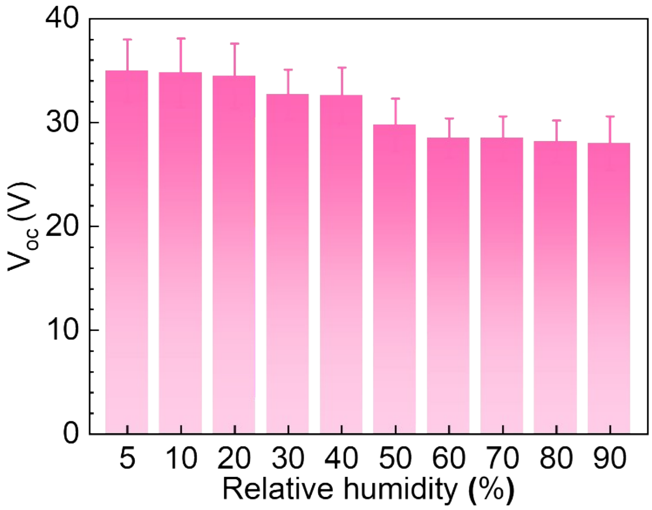

Fig. S22 | The influence of environmental humidity on the electrical output of WDPs.

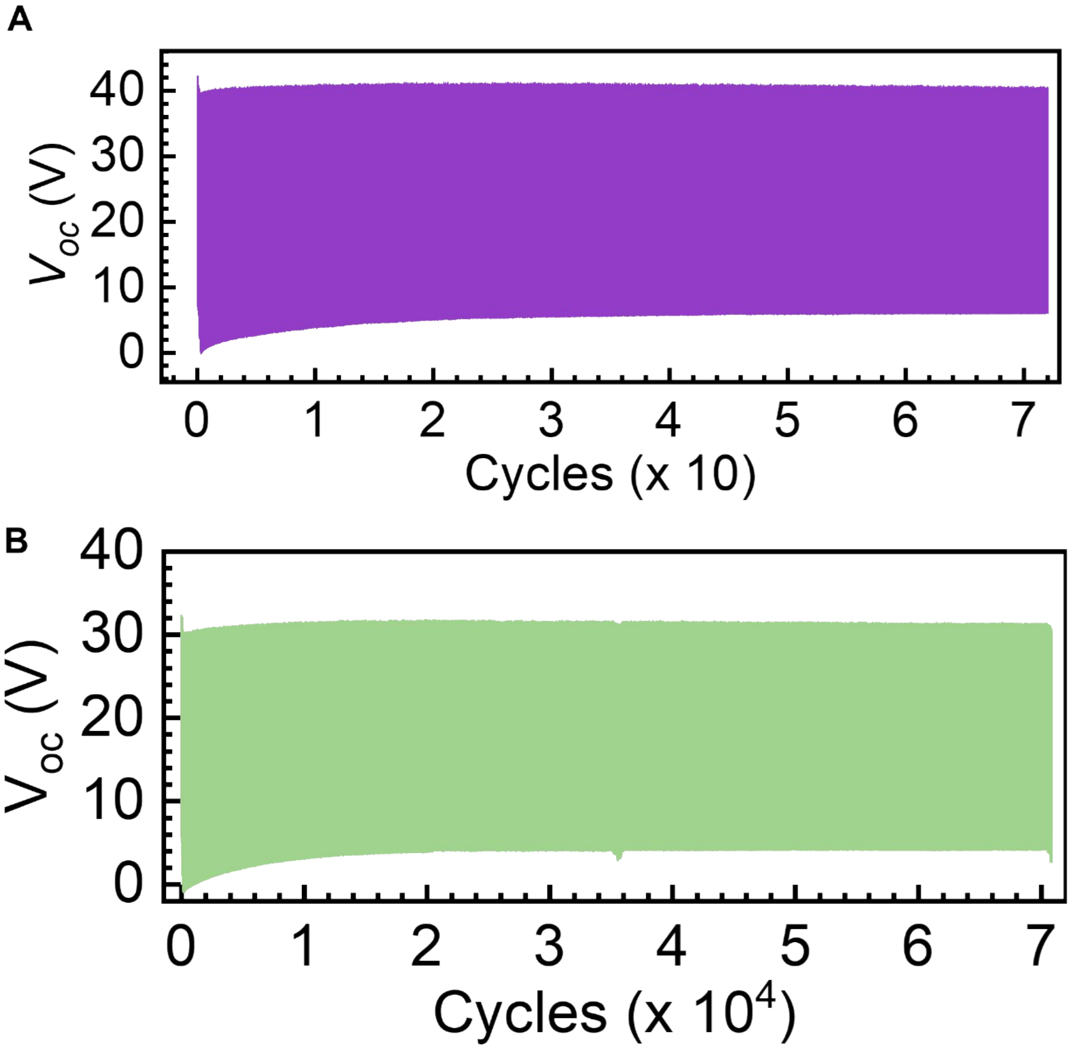

Fig. S23 | **(A)** The durability test of WDPs in compression state. **(B)** The durability test of WDPs in tensile state.

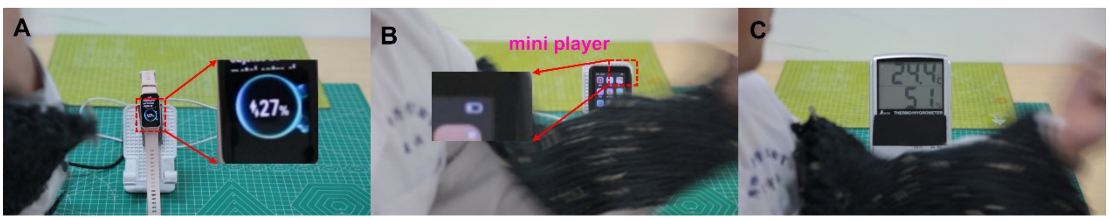

Fig. S24 | The demonstration of driving a smart bracelet, a mini player and a thermohygrometer.

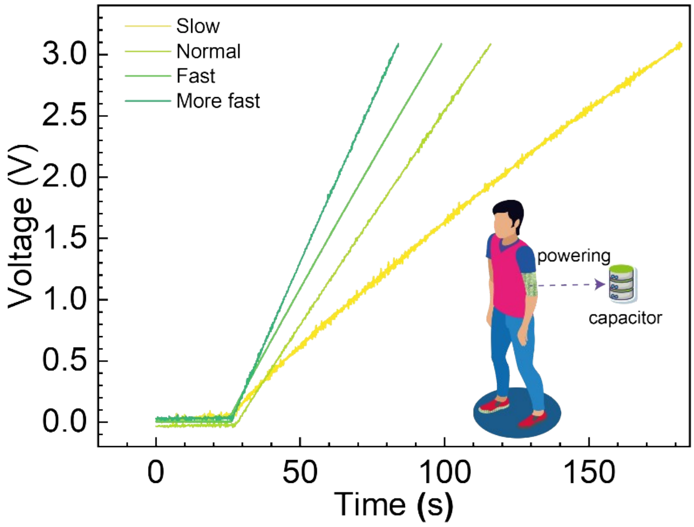

Fig. S25｜The charging characteristics of WDPs with1 mF capacitor by harvesting biokinetic energies at different bending speeds.

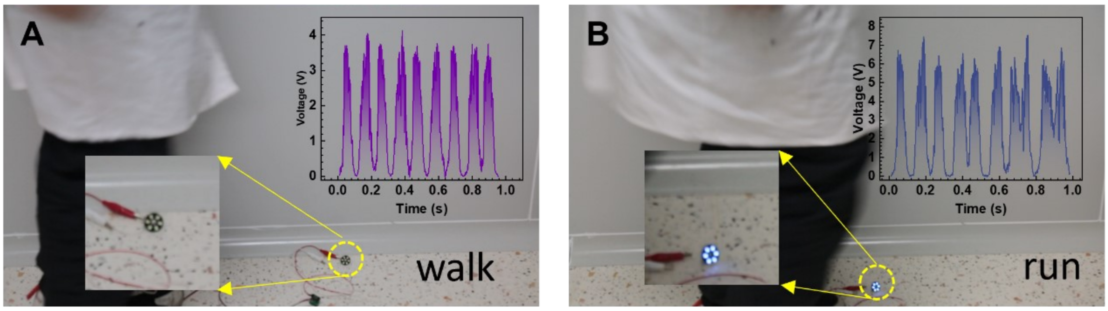

Fig. S26｜ (A, B) The voltage generated by WDP under walking and running.

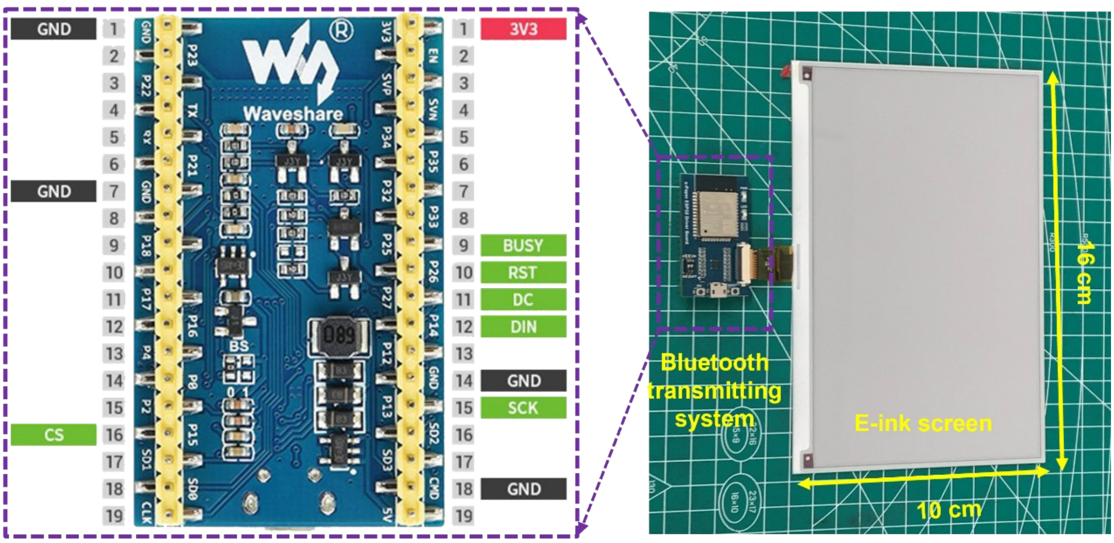

Fig. S27｜The bluetooth transmitting system and e-ink screen.

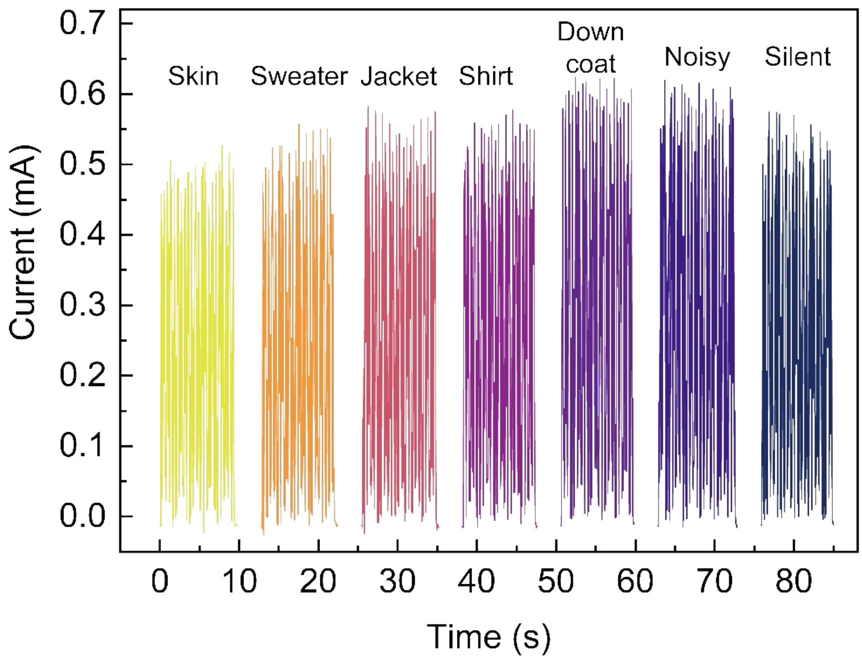

Fig. S28 | The output of WDP on skin and different clothing materials.

Table 1 The performance of different type TVNGs and TENGs

Material	TVNG/ TENG	DC/ AC	Textile	Hydrop hobic	Flexi bility	Stretc habili ty	V_{oc} (V)	Power density (W/m^2)	Resistance (MΩ)	Durability (Cycles)	Refere nce
Cu/PTFE	TENG	AC	✓	×	✓	×	6	1.25×10^{-3}	10	—	11
CNT/PTFE	TENG	AC	✓	×	✓	×	20	4×10^{-3}	1000	10000	18
Ag/PTFE	TENG	AC	✓	×	✓	×	900	2×10^{-3}	100	—	22
Water/PTFE	TENG	AC	×	✓	×	×	150	50.1	0.3	—	32
Ag/PDMS	TENG	AC	✓	×	✓	✓	48	—	2000	—	12
Graphene/ PDMS	TENG	AC	✓	×	✓	×	70	30×10^{-3}	100	—	23
PE/PDMS	TENG	AC	✓	✓	✓	✓	200	0.8×10^{-3}	1000	5700	21
Ag/PDMS	TENG	AC	✓	×	✓	✓	20	22×10^{-6}	150	1800	27
Conductive yarn/PI	TENG	AC	✓	✓	✓	✓	140	70×10^{-6}	1000	—	25
Conductive	TENG	AC	✓	✓	✓	✓	0.12	0.12	10	1000	29

polyamide/PI											
Bi_2Te_3/Kapton	TENG	AC	×	×	×	×	50	—	30	—	17
Ag/PE	TENG	AC	✓	×	×	✓	40	10.5×10^{-3}	1000	10000	28
Ag/Nylon	TENG	AC	✓	×	✓	✓	20	2.2×10^{-3}	20	10000	20
Ag/EP	TENG	AC	✓	×	×	✓	18	0.7	24	—	24
Conductive yarn/PAN:PVDF	TENG	AC	✓	✓	✓		30	350×10^{-6}	500	—	26
n-SWCNT/ p-SWCNT	TVNG	DC	✓	×	×	×	0.3	—	3.3	1280	47
GaN/Bi_2Te_3	TVNG	DC	×	×	×	×	48	11.85	0.16	—	53
MoS_2/Ta_4C_3	TVNG	DC	✓	×	✓	×	0.3	37×10^{-3}	0.55	54000	41
Al/PEDOT:PSS	TVNG	DC	✓	×	✓	×	0.6	—	—	4000	33
Al/PEDOT:PSS	TVNG	DC	×	×	✓	×	2	—	0.2	20000	34
Al/PEDOT:PSS	TVNG	DC	✓	×	✓	×	0.45	1.2×10^{-3}	30	3350	42
Al/PEDOT:PSS	TVNG	DC	✓	×	✓	×	0.8	0.13	0.01	5000	43
Al/PPy	TVNG	DC	✓	×	×	×	0.4	0.17	0.43	20000	45
Au/PPy	TVNG	DC	×	×	✓	×	0.7	0.15	0.0082	—	46
PBFD/ PEDOT:PF	TVNG	DC	✓	✓	✓	✓	40	1.05	0.035	72000	This work

Video.S1. The V_{oc} of WDPs.

Video.S2. The I_{sc} of WDPs.

Video.S3. The WDPs charge a commercial lithium-ion battery at 5 Hz.

Video.S4. The WDPs charge drive the 25, 32, and 40 V colored electric lamps at 3 Hz, 4Hz and 5 Hz.

Video.S5. The WDPs drive the 3, 10, and 20 V colored lights by harvesting the kinetic energy of the human body.

Video.S6. The WDPs drive a 25 mW mobile phone, a10 mW smart bracelet and a 8 mW thermo-hygrometer by harvesting the kinetic energy of the human body.

Video.S7. The WDPs charge a 1 mF capacitor by harvesting the kinetic energy of the human body.

Video.S8. The WDPs drive the bluetooth transmitting system (Fig. S27) and the e-ink screen.